Self-Organized UWB Localization for Robotic Swarm – First Results from an Analogue Mission on Volcano Etna

**Siwei Zhang, Pedro Fernandez Ruz,
Fabio Broghammer, Emanuel Staudinger,
Christian Gentner, Robert Pöhlmann, Armin Dammann
Institute of Communications and Navigation
German Aerospace Center (DLR)
Münchener Str. 20, 82234-Wessling, Germany
Siwei.Zhang@dlr.de**

**Manuel Schütt, Roy Lichtenheldt
Institute of System Dynamics and Control
German Aerospace Center (DLR)
Münchener Str. 20, 82234-Wessling, Germany**

***Abstract*—At the Institute of Communications and Navigation of the German Aerospace Center (DLR), we have studied and developed radio-based swarm navigation technologies for a decade. In this paper, we provide a complete solution of ultra-wide band (UWB) localization network for a robotic swarm. This network is organized in a fully decentralized fashion and resilient to clock imperfections, topology changes, packet loss and the hidden node problem. In this network, a multitude of active devices and an arbitrary number of passive devices can exploit the UWB signals for self-localization, i.e. estimating their relative positions and orientations, without sophisticated clock and antenna calibration, which dramatically simplifies the design and manufacturing of such a swarm. Our proposed solution is verified with experiments and was successfully demonstrated in a space-analogue multi-robot surface exploration mission on the volcano Mt. Etna, Sicily, Italy, in July 2022.**

TABLE OF CONTENTS

1. INTRODUCTION 1
2. ULTRA-WIDE BAND (UWB) FOR SWARM 2
3. SELF-ORGANIZED SWARM NETWORK 3
4. PROPAGATION TIME-BASED OBSERVATIONS 4
5. POSITION AND ORIENTATION ESTIMATION 6
6. SPACE-ANALOGUE MISSION ON VOLCANO ETNA 7
7. CONCLUSION 9
ACKNOWLEDGMENTS 9
REFERENCES 9
BIOGRAPHY 10

1. INTRODUCTION

A swarm of robots can rapidly explore challenging extraterrestrial environments, such as lunar caves or Martian canyons [1]. For example, in the conceptual extraterrestrial surface and lava tube exploration mission depicted in Figure 1, a swarm of crawlers depart from the landing side, deploy sensor boxes and collaboratively explore a lava tube under the extraterrestrial surface. Compared to a single robot, a swarm can make simultaneous observations at different locations and avoids a single point of failure, which leads to a paradigm shift in exploration missions [2]. For the success of an autonomous swarm mission, reliable communication and navigation within the swarm is mandatory [3]. Research has been intensively conducted in related fields, e.g. self-organized networks [4], ultra-wide band (UWB) ranging [5] and network localization [6, 7]. However, there is little guidance on the system-level design of such a communication and navigation network for a real-world robotic swarm.

978-1-6654-9032-0/23/$31.00 ©2023 IEEE

At the Institute of Communications and Navigation of the DLR, we have studied and developed radio-based swarm navigation technologies for a decade. In [8], we investigated the hidden node problem while establishing a swarm network with self-organized time-division multiple access (SOTDMA) schemes. In [9], we studied the fundamental limit of ranging and localization in a swarm with limited radio resources. In [10], we proposed a novel distributed particle filter (DPF) for swarm localization and extended it for joint position and orientation estimation in [11] by fusing range measurements with inertial measurement unit (IMU) data and control commands. In [1], we proposed information seeking formation optimization to improve swarm navigation, and we examined the impact of imperfect clocks on swarm navigation in [12]. In [13], we described the system integration of the software-defined radio (SDR)-based swarm navigation platform developed at DLR.

In this paper, we demonstrate step-by-step how to design a self-organized swarm localization network employing low-cost and light-weight UWB devices. This network is organized in a decentralized fashion, adapting itself to topology changes caused by splitting and rejoining of the swarm. A multitude of active devices, which transmit and receive UWB signals, and an arbitrary number of passive devices, which can only receive signals, can exploit the network for self-localization, i.e. estimating their positions and orientations relative to the swarm. Due to the dense mesh network nature of the swarm, the system imperfections like clock drifts and antenna delays can be calibrated simultaneously with localization, which dramatically simplifies the design and manufacturing of the robotic swarm.

We start from evaluating the clock characteristics of the low-cost UWB devices and discover that the stability of the UWB clocks are orders of magnitude worse than the temperature controlled crystal oscillators (TCXOs) used in our SDR-based swarm platform. Then, we propose a SOTDMA protocol based on the DESYNC algorithm [4, 8]. The modified protocol is robust against network dynamics, packet loss, hidden node problems, etc., and has great potential for spectrum spatial reuse. Therefore, it is particularly suitable for a large-scale swarm. After a SOTDMA swarm network is established, we study localization-related observations at both active and passive nodes, accounting for the clock imperfections. An important contribution here is the passive node time difference of arrival (TDoA) observations, eliminating the clock offsets and drifts. These observations enable localization of an arbitrary number of passive nodes. Thanks to their compact size and high ranging accuracy, multiple UWB devices can be mounted on a single robot for joint position

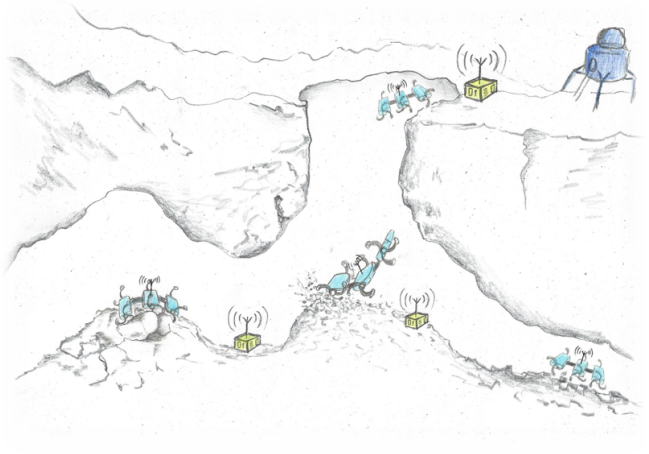

Figure 1: A conceptual extraterrestrial surface and lava tube exploration mission.

Figure 2: Qorvo UWB devices and two rovers built at DLR for indoor experiments.

and orientation estimation of the robot. For the estimation, we propose a modified DPF based on the algorithms introduced in [10].

In July 2022, we successfully demonstrated our self-organized UWB swarm localization technology in a space-analogue surface exploration mission on volcano Mt. Etna, Sicily, Italy [14], within the Helmholtz Future Project ARCHES. In this mission, a wheeled rover, a six-legged cave crawler, and a hexacopter, each equipped with four UWB devices, performed coordinated maneuver, while their positions and orientations are precisely estimated with our localization network.

This paper provides a complete picture of our methods, system design and first results from the analogue mission, which sheds light on the usage of UWB for joint communication and navigation in a robotic swarm for future exploration missions.

2. Ultra-Wide Band (UWB) for Swarm

A radio signal is considered as UWB if the -10 dB fractional bandwidth is greater than 0.2 or if it occupies at least 500 MHz of the spectrum [15]. On Earth, UWB is often used as secondary application with low power, to reduce interference on primary applications like cellular networks and global navigation satellite system (GNSS) receivers. The large bandwidth of UWB provides high temporal resolution of the channel impulse response, which enables precise propagation time-based localization in complex multi-path environments [5, 16], such as lunar caves or Martian canyons. As an example, with the up to 900 MHz bandwidth provided by IEEE 802.15.4a compliant UWB devices, the line-of-sight (LOS) path can be separated from multi-paths that are one decimeter longer than the LOS path. As a comparison, a typical GNSS signal has a bandwidth of 24 MHz (e.g. GPS L1) to 46 MHz (e.g. Galileo E1), which is vulnerable to multi-paths that are meters longer than the LOS path. In recent years, light-weight, low-cost and easy to program UWB chips, like the ones from the company Qorvo, have been manufactured for a wide spectrum of industrial and logistic applications that demand centimeter-level localization accuracy. Even though the methodology proposed in this paper is generic, we use the DWM1001-DEV modules [17] from Qorvo as an example for implementing the self-organized localization framework for our robotic swarm applications, as shown in Figure 2.

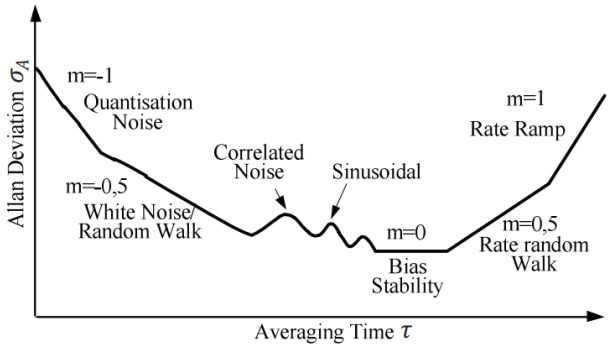

Figure 3: Allan Deviation regions [19].

Clock Evaluation

For a large-scale localization network, the timing information plays an essential role [12]. First, the nodes in a network coordinate their transmission time to avoid package collisions. Second, accurate propagation time needs to be obtained for precise localization. Therefore, as the first step of the system design, we evaluate the characteristics of the low-cost clocks embedded in UWB devices.

The clock characteristics can be separated into long-term and short-term behavior, which are described by a mathematical expression called Allan Deviation [18]. Different regions of the Allan Deviation curve of a clock are illustrated in Figure 3. For our application, in order to capture the dynamics of the network, a short SOTDMA period, in the order of 100 ms, is required. Therefore, we focus on the short-term behavior of the clock, governed by the quantization and phase noise. In order to calculate the Allan Deviation of the UWB clocks, we setup an experiment with three static devices as shown in Figure 4, collecting time of arrival (ToA) measurements between every pairs for three days. In Figure 5, we compare the Allan Deviation of the UWB clocks with the ones of other clocks, namely TCXO, micro electromechanical systems (MEMS) clock, oven controlled crystal oscillator (OCXO) and Rubidium atomic clock. The

Figure 4: Setup for Allan Deviation experiment.

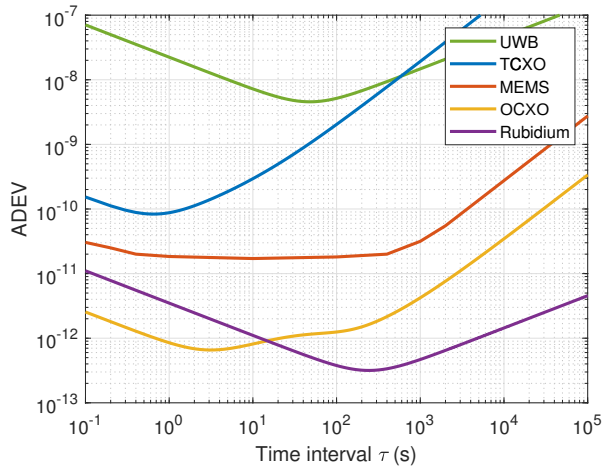

Figure 5: Allan Deviation comparison between the measured UWB clocks and other types of clocks reported in [20].

TCXO is measured in our lab at DLR and the Rubidium atomic clock is generated with clock models from literature [12]. The UWB clocks are roughly three orders of magnitude worse than TCXO in the short-term, which means that the clock imperfection needs to be compensated for localization but can be neglected when designing a SOTDMA protocol.

3. Self-Organized Swarm Network

Self-Organized Time Division Multiple Access (SOTDMA)

Network protocols for swarms require flexibility to adapt the changing topology and formation of the swarm. The adaptation has to be achieved quickly to support high dynamics. Furthermore, these protocols should be fully decentralized in order to avoid a single point of failure. Therefore, we design a SOTDMA protocol based on the DESYNC algorithm proposed in [4].

DESYNC employs the concept of pulse coupled oscillator (PCO) [21], where every node in the network tries to separate its transmission time from the others. Each node adjusts its transmission phase, i.e. the modulo transmission time normalized to a time-division multiple access (TDMA) period, towards the middle point between its temporal neighbors. An example of DESYNC is illustrated in Figure 6. The red node i adjusts its transmission phase at a TDMA frame t by observing the transmission phases of its predecessor $\phi_{i+1}(t)$

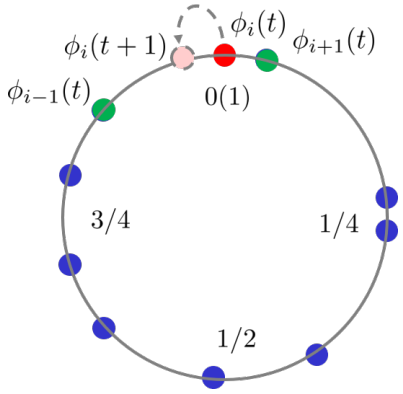

Figure 6: DESYNC protocol example.

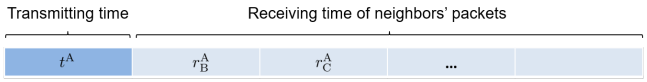

Figure 7: Payload data format of a generic node A.

and successor $\phi_{i-1}(t)$ marked in green:

$$\phi_i(t+1) = \frac{\alpha}{2}\big(\phi_{i-1}(t) + \phi_{i+1}(t)\big) + (1-\alpha)\phi_i(t). \quad (1)$$

The network is proven to be stable when the forgetting factor $\alpha \in (0, 1)$ [4]. DESYNC comes with two major advantages. Firstly, no central clock is required as every node tracks the cycle independently. Secondly, there is no pre-defined schedule, so that it can support any number of agents to join or leave the network, suitable for dynamic scenarios. Two unaddressed problems of DESYNC are packet loss and hidden nodes. To solve these problems, we first design payload data carried by the transmitted signals of a generic node A as shown in Figure 7. The payload data contains the scheduled transmission time t^A, and the receiving local time $r_B^A, r_C^A, \ldots$ of the latest data from neighbors $B, C, \ldots$.

Packet Loss Problem

In a dynamic network, packet loss can occur in the case of low signal to noise ratio (SNR) or transmission collisions. Frequent packet losses of one node may force other nodes to react on this change and jeopardize the stability of the whole network. Our proposed payload data structure can inherently reduce the chance of packet loss. The information of temporal neighbors can be obtained not only from these neighbors, i.e. reading t^A in the example in Figure 7, but also from the data transmitted by other nodes, i.e. reading $r_B^A, r_C^A, \ldots$. In addition, we introduce memory into the network protocol. Each node has a fixed time memory of its direct temporal neighbors. Instead of adapting its transmission phase based on the two current neighbors, the node searches in its memory to find the nearest predecessor and successor as its direct neighbors. This approach reduces the sensitivity to network changes, but at the cost of an increased reaction time. We conducted a similar experiment as in Figure 4, with a reduced transmission power to test SOTDMA with the presence of significant packet loss. Figure 8a shows the transmission phases of node 0, 1, and 2 with respect to (w.r.t.) the initial phase of node 0, with the standard DESYNC. It can be seen that the SOTDMA slot structure is unstable. By adding a memory, the modified DESYNC leads to a much more stable SOTDMA slot structure as shown in Figure 8b.

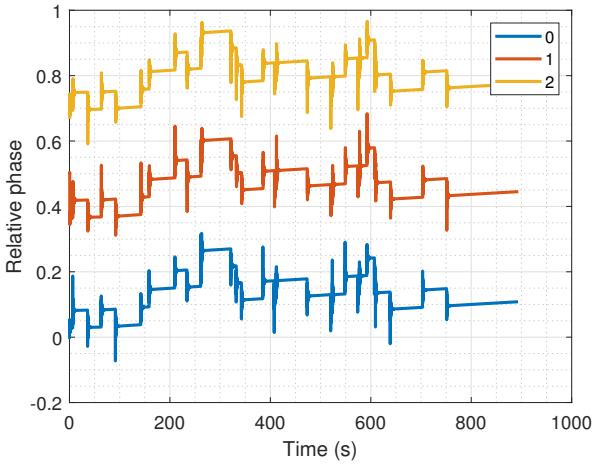

(a) Relative phases without memory.

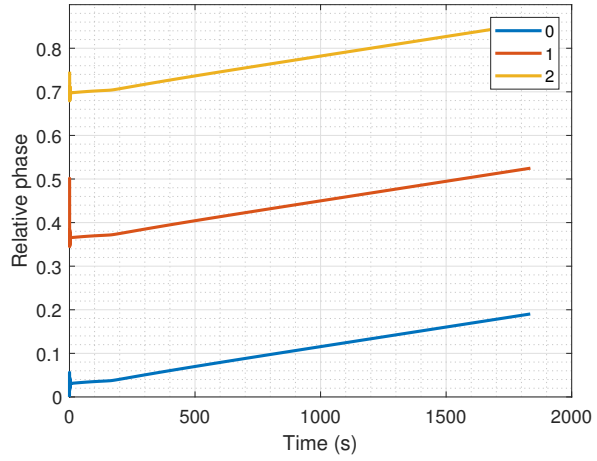

(b) Relative phases with memory.

Figure 8: Indoor experiment of three nodes SOTDMA establishment with a setup similar to Figure 4: Transmission phases of the nodes w.r.t. the initial phase of node 0 are depicted, with/out memory.

Hidden-Node Problem

The hidden node problem happens when two nodes have no direct communication link but share a common neighbor, as illustrated in Figure 9. In this example, packets from node B and C may be transmitted at the same time, which leads to a collision at node A. This problem can also be solved by our proposed payload structure. By decoding the data packets from its neighbors, a node gets access to the information of its two-hop topological neighbors. When deciding a transmission phase, the node takes all its one- and two-hop topological neighbors into account. Therefore, avoiding collision at its one-hop neighbors. We conducted a new experiment to test the hidden node scenario. A setup with five nodes is presented in Figure 10. The transmission power is adjusted so that the network topology is as indicated with white edges. The emerging SOTDMA structure can be seen in Figure 11, where the transmission phases are plotted. The inner ring includes node 0 and its detected direct topological neighbors, i.e. node 1 and 4. The middle ring additionally includes the detected two-hop neighbor, i.e. node 2. Hence, in this view, the SOTDMA slots are uniformly spaced. The outer ring shows the global view on the transmission. In this sparsely connected network, we can see that nodes are able to coordinate their transmissions to avoid collisions, even though the global SOTDMA slots are no longer uniformly spaced. It is worth to mention that by the proposed modification, three-hop neighbors are allowed to use the same SOTDMA slot. This spatial reuse feature is particularly beneficial for a large-scale swarm.

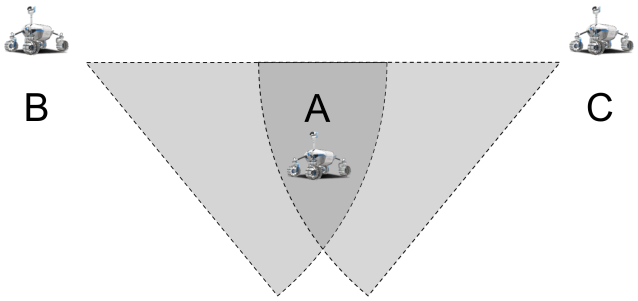

Figure 9: Hidden node scenario in a network with three devices.

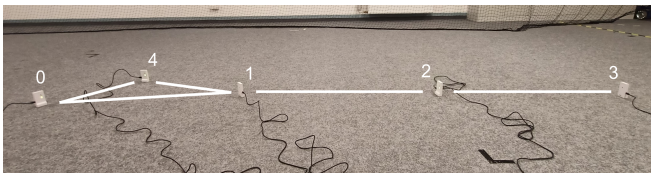

Figure 10: Hidden node setup with links indicated in white.

4. Propagation Time-Based Observations

After self-organizing the network, nodes can exploit the network for localization with propagation time-based observations. As we discussed in Section 2, with the UWB signal, the LOS path can be separated from multi-paths that are one decimeter longer than the LOS path. Therefore, we ignore the multi-path propagation in this paper and focus on the clock imperfection. This treatment is validated later by indoor measurements. The SOTDMA structure imposes a maximum number of active nodes in the network. However, with the observations from passive nodes, the number of localizable nodes becomes virtually infinity, similar as in GNSSs, except the clock drifts at both transmitter and receiver sides need to be considered. Since only the short-term behavior in the range of sub-second of the clock is relevant, we use a simplified clock model, for a generic node A:

$$t^A = \delta^A t + \mu^A, \tag{2}$$

stating the observed time t^A at node A is the true time t multiplied by a constant drift δ^A which is close to one, and added with a constant offset μ^A. For this investigation, we omit the clock noise and focus on the impact of the clock offset and drift. We use the network illustrated in Figure 12 with packet exchange diagram shown in Figure 13 to demonstrate three methods to obtain time-based observations. A exchange between two active nodes A and B with a passive node E are depicted in Figure 13 with B as the initiator.

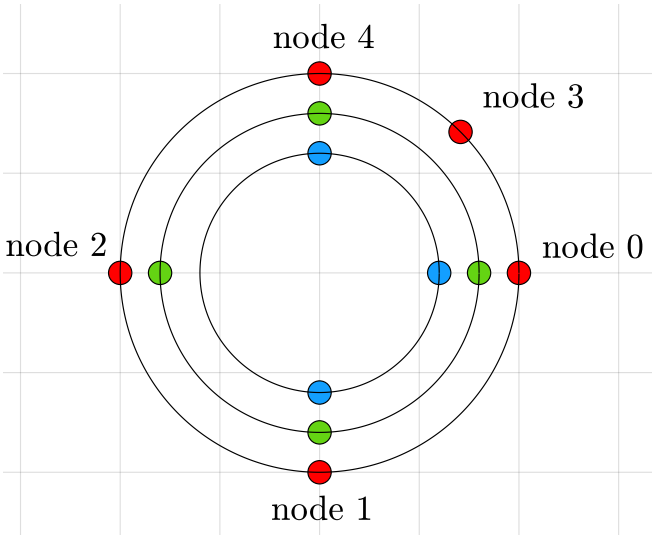

Figure 11: Emerging SOTDMA slots with the hidden node setup.

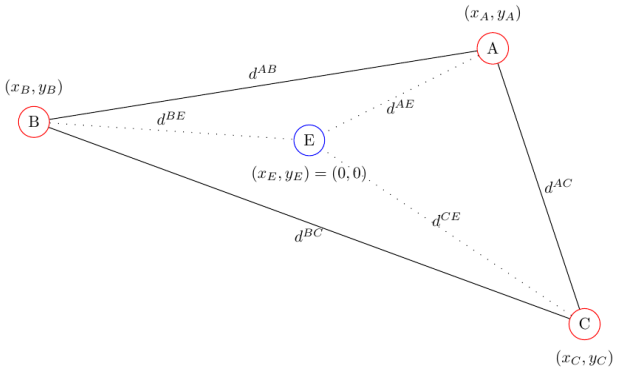

Figure 12: Network of three active nodes A, B, C and a passive node E.

Three-Way Ranging between Active Nodes

One-way ranging, i.e. ToA measurement assumes perfect synchronization between both clocks, which is not realistic in most applications. The most commonly used network ranging protocol is two-way ranging, which is preferable for quick reply (small Δ^B) normally associated with a unicast protocol, or a very precise clock with a negligible drift. The ranging error is approximated as

$$\epsilon^{AB}_{RTT} \approx \frac{c\Delta^B(\delta^A - \delta^B)}{2\delta^B}. \tag{3}$$

In our typical SOTDMA setup with low-cost UWB devices, i.e. $\Delta^B > 10$ ms and $\delta^A - 1, \delta^B - 1$ around 10 ppm, the ranging error is larger than 30 m. We define

$$T^X = r_3^X - r_1^X, \quad X \in \{A, B, C, E\}. \tag{4}$$

The three-way ranging method can be applied to get the distance estimate between two active nodes [17], for example nodes A and B as

$$\hat{d}^{AB} = c\frac{RTT^A \cdot RTT^B - \Delta^A \cdot \Delta^B}{T^A + T^B}. \tag{5}$$

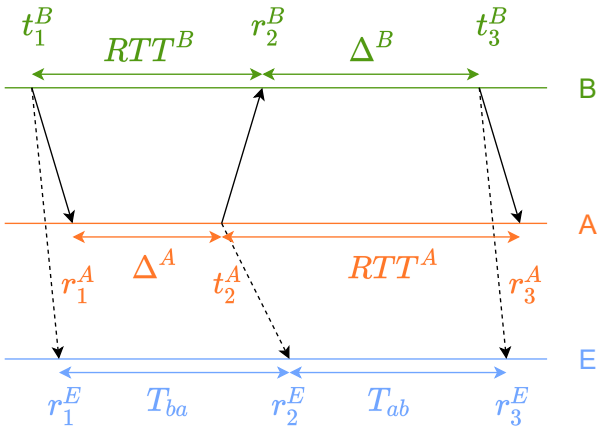

Figure 13: Time diagram for a three-way ranging packet exchange between nodes A and B with a additional passive node E.

The clock drift related ranging error is approximated as

$$\epsilon^{AB} \approx d^{AB}\left(\frac{\delta^A + \delta^B}{2} - 1\right). \tag{6}$$

Eavesdropping Ranging at Passive Nodes

Thanks to the payload data format defined in Figure 7, a passive node E can estimate distance d^{AB} between two active nodes A and B:

$$\hat{d}^{AB}_E = \frac{1}{2}\left(\frac{T_{ba}T^A}{T^E} - \Delta^A\right) + \frac{1}{2}\left(\frac{T_{ab}T^B}{T^E} - \Delta^B\right), \tag{7}$$

with a drift related error of

$$\epsilon^{AB}_E \approx \left(\frac{\delta^A + \delta^B}{2} - 1\right) d^{AB}. \tag{8}$$

This approach is useful for a heterogeneous swarm with unbalanced computational resources. A few passive (or active) nodes can collect distance information of active nodes and localize a subset of the swarm.

Time Difference of Arrival (TDoA) at Passive Nodes

One highlight of our approach is the localizability of a passive node E by observing the TDoA from two active nodes A and B. TDoA is defined as

$$D^{AB}_E = d^{AE} - d^{BE}. \tag{9}$$

The estimated TDoA can be obtained by

$$\hat{D}^{AB}_E = \frac{1}{2}\left(\frac{T_{ba}T^A}{T^E} - \Delta^A\right) - \frac{1}{2}\left(\frac{T_{ab}T^B}{T^E} - \Delta^B\right), \tag{10}$$

where the drift related error is approximated as

$$\epsilon^{ABE}_E \approx \left(\frac{\delta^A + \delta^B}{2} - 1\right)\left(d^{AE} - d^{BE}\right). \tag{11}$$

With our typical scenario, a swarm spans an area of 100 m $\times$ 100 m. The drift increments $\delta^A - 1$ and $\delta^B - 1$ are in the order of 10 ppm as the UWB clocks we evaluated. The clock drift related ranging errors for active nodes three-way ranging (6), passives node eavesdropping ranging (8) and passive nodes TDoA (11) are in the range of 1 mm, which is negligible.

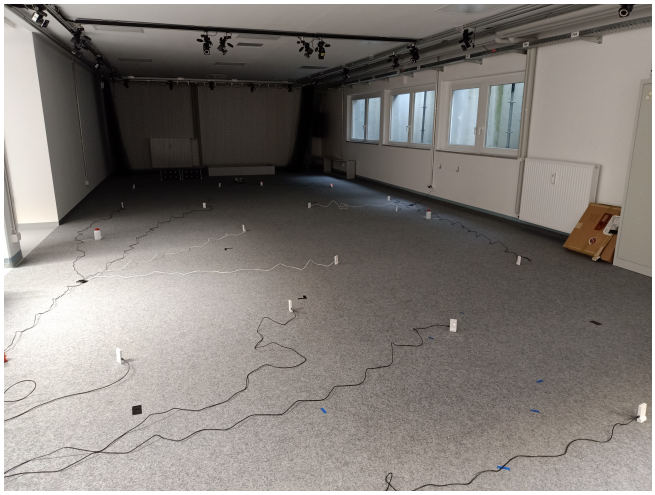

(a) Experimental setup in the holodeck: static nodes are deployed on the ground. The positions of all nodes are tracked by the optical tracking system mounted on the ceiling.

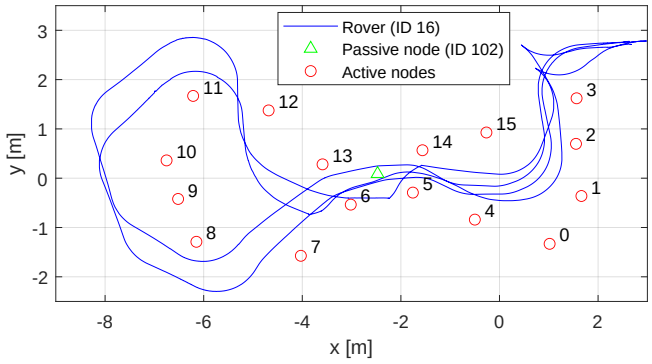

(b) Recorded ground-truth positions of 16 active static nodes, one passive static node and one mobile node mounted on a DLR rover shown in Figure 2.

Figure 14: Indoor measurement in the holodeck of DLR.

Experimental Verification in the Holodeck

We conducted propagation time-based measurements in the holodeck at DLR, where 16 static active nodes, one moving active node on rover and one passive node are deployed. Real-time positions are tracked by the optical tracking system mounted on the ceiling. The measurement setup is shown in Figure 14a and the recorded ground-truth positions of the nodes in Figure 14b. For this experiment, 272 ranging links are updated every $T = 100$ ms. Figure 15 shows the three-way ranging results compared to the ground-truth distance between static node 0 and moving node 16. It can be observed that the estimate coincides with the true distance well, except for a few sub-meter spikes at large distances, which are caused by low SNR and multi-path propagation. This result shows that the designed UWB network is suitable for complex multi-path environments.

The passive node TDoA performance is showcased in Figure 16, where the TDoA is calculated between node 0 and node $X \in \{1, 3, 7, 13\}$ at the passive node 102, i.e.

$$D_{102}^{0,X} = d^{0,102} - d^{X,102} = \|\mathbf{p_0} - \mathbf{p_{102}}\| - \|\mathbf{p_X} - \mathbf{p_{102}}\|, \quad (12)$$

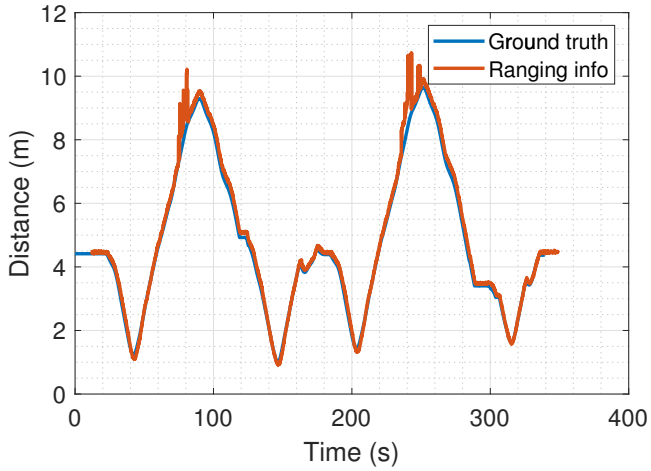

Figure 15: Three-way ranging results between the active static node 0 and the mobile node 16, in comparison with the distances calculated from the recorded ground-truth positions.

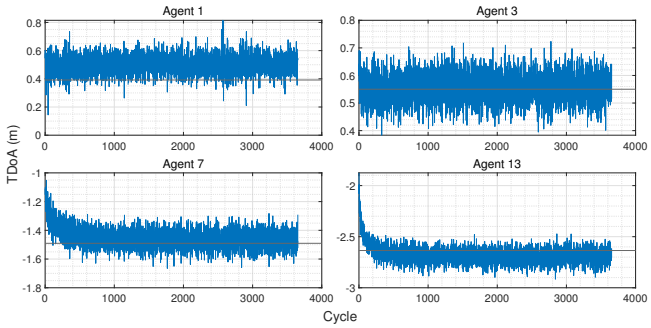

Figure 16: Passive node TDoA performance with node 0 as a common reference.

where $\mathbf{p_A}$ denotes the position of a generic node A. The true TDoAs are indicated with horizontal black lines. It can be seen that the TDoA observations coincide with the true values with a white noise level of 10 cm, which is similar as the noise level of the active node three-way ranging. For node 1, there is an additional bias of around 10 cm, which is from the delay of the radio frequency (RF) chain.

5. Position and Orientation Estimation

Once the propagation time-based observations have been obtained, robots in the swarm are ready to estimate their positions. For robots equipped with multiple UWB devices, additional orientation information can be acquired. At DLR, DPF has been developed for swarm localization [10, 11], which can be extended to UWB-based localization. For robots with multiple UWB devices, instead of describing localization algorithms in detail, we only introduce two design concepts of DPFs. The first approach is to consider each UWB device as an agent in the network. In this case, only the positions of the agents need to be estimated for example by the DPF in [10, 11]. Then, those positions can be transformed into the positions and orientations of the robots given the mounting geometry of the UWB devices. The second approach is to assign a DPF to each robot, whose state includes the position and orientation of the robot. Firstly, the

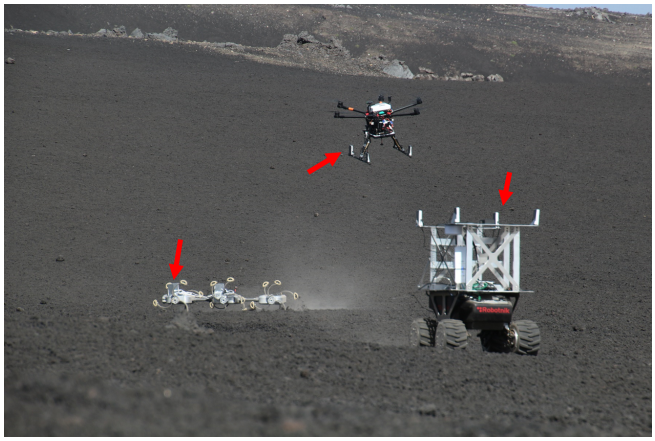

Figure 17: Mission scenario on Mt. Etna robots with attached UWB devices.

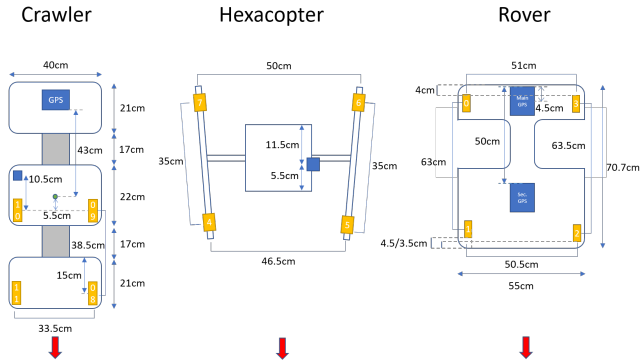

Figure 18: Top-view blueprints of robots with attached UWB devices.

mounting geometry of the UWB devices is used to estimate the RF delays of the devices. Then, position and orientation of the robot can be directly estimated by the DPF. In this way, the bias from the RF delay is eliminated. The impact of white measurement noise is reduced by Bayesian tracking. Therefore, high precision localization can be achieved.

6. Space-Analogue Mission on Volcano Etna

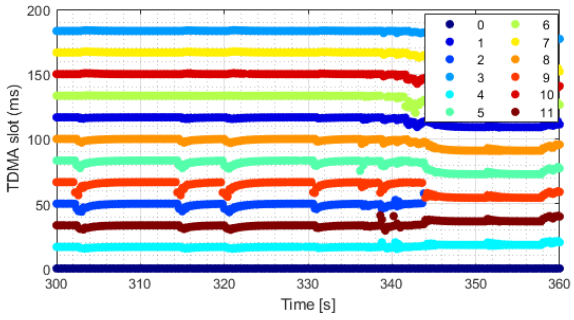

Figure 19: TDMA slots recorded at node 0.

In July 2022, we successfully demonstrated our self-organized UWB swarm localization technology in a space-analogue surface exploration mission, on the volcano Mt. Etna, Sicily, Italy [14]. Figure 17 shows the setup of the mission. The robots are, from left to right: a lunar cave crawler built by the Institute of System Dynamics and Control at DLR, a commercial hexacopter and a commercial rover, both from the Institute of Communications and Navigation at DLR. Each robot is equipped with four UWB devices highlighted in Figure 17. The displacement of the UWB devices is depicted in Figure 18. The three robots performed coordinated maneuver in 3D, while their positions and orientations are precisely estimated with our network localization. All 12 UWB devices are active nodes, but only nodes 0 to 3 on the rover record data packets, which can obtain active three-way ranging, eavesdrop three-way ranging and conduct passive TDoA from other pairs.

The thorough post-processing of the collected data is still ongoing. However, preliminary results already look promising. The observations recorded at node 0 are presented.

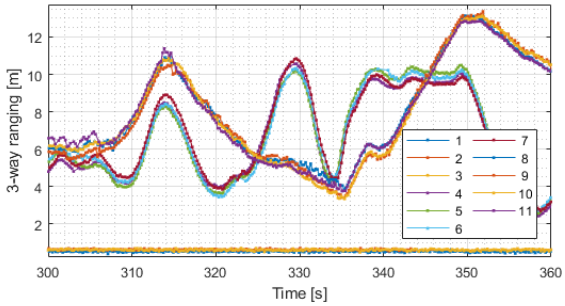

Figure 20: three-way ranging recorded at node 0.

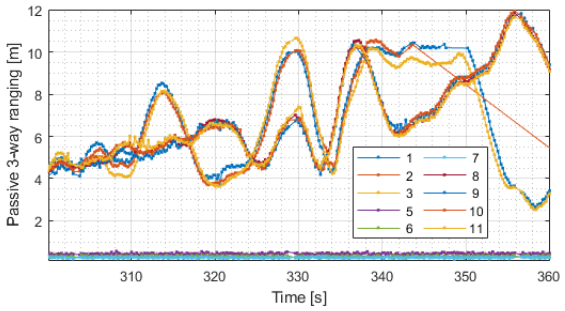

Figure 21: Passive three-way ranging $d^{4,X}$ between node 4 and another node $X \notin \{0, 4\}$, recorded at node 0.

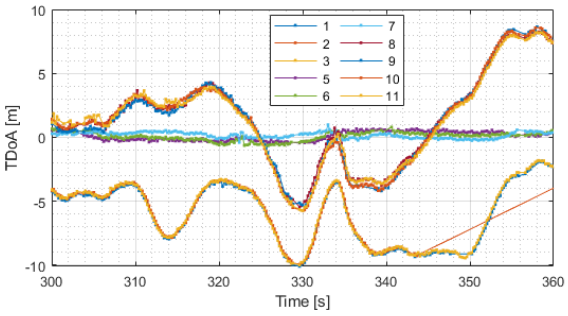

Figure 22: TDoA $D_0^{4,X}$ between node 4 and another node $X \notin \{0, 4\}$, recorded at node 0.

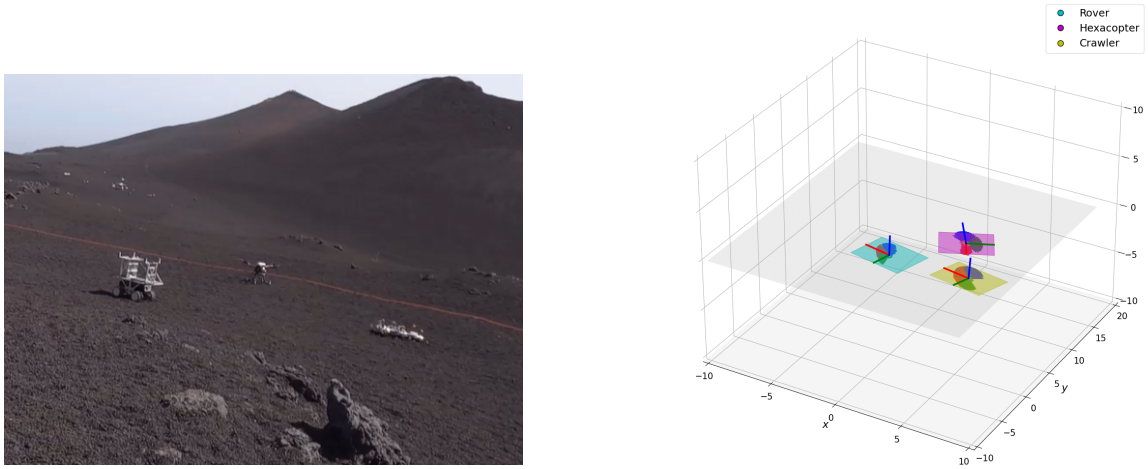

Figure 23: 3D position and orientation estimation at 8 s.

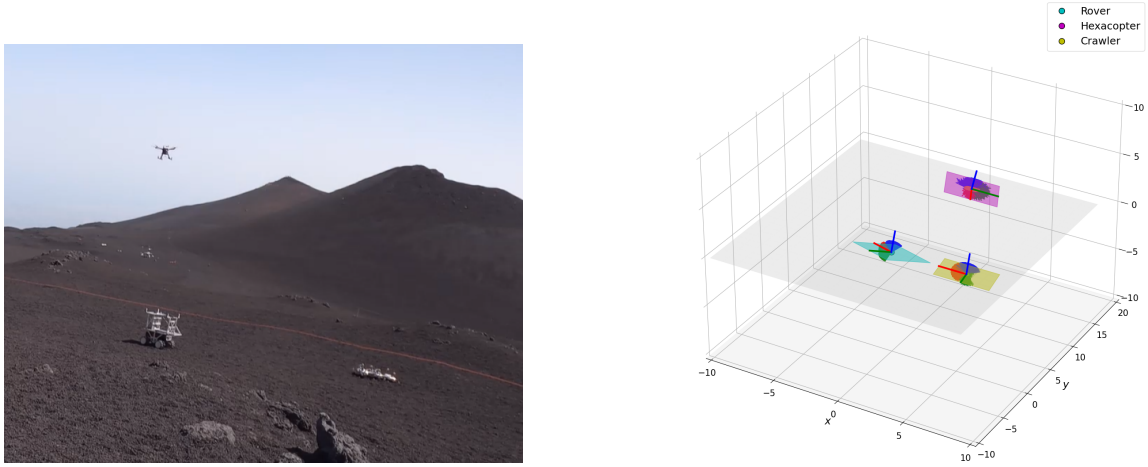

Figure 24: 3D position and orientation estimation at 254 s.

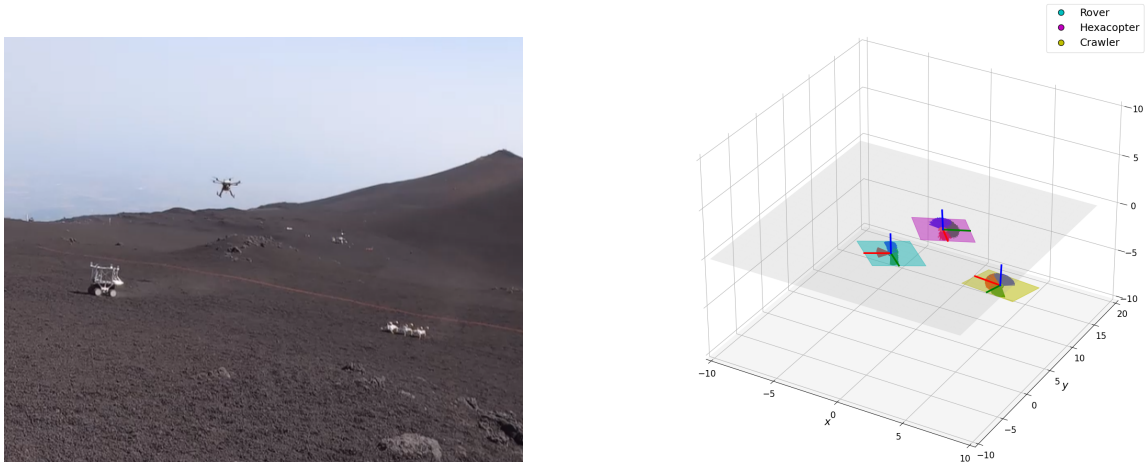

Figure 25: 3D position and orientation estimation at 280 s.

Figure 19 illustrates the emerging SOTDMA slot structure observed at node 0, which shows that the structure is adaptive to changes of the network topology and can re-stabilize itself. Figure 20, Figure 21 and Figure 22 show the performance of active three-way ranging, eavesdrop three-way ranging and passive TDoA, respectively. We can see these propagation time-based observations are varying smoothly following the robots' dynamics and are clustered into three groups, corresponding to the three robots. In addition, when node 0 is considered as a passive node, see Figure 21 and Figure 22, there is discontinuity in the measurements involving node 4 and node 2. As there is no link between nodes 2 and 4, the

calculation of (7) and (10) is impossible. Since every robot has four points with known relative positions that exchange ranging information, the orientation is observable. In order to determine the orientation, a DPF designed according to the second approach from Section 5 is applied. Each DPF combines not only ranging measurements directly collected at the rover, but also eavesdropped three-way ranging between crawler and hexacopter, and estimates the robot position and orientation jointly. Since it is an anchor-free scenario in 3D, six constraints have to be included to uniquely determine a reference frame. For that, we constrain the rover at the origin, the crawler on the positive x-axis and the hexacopter on the x-y plane. Figure 23, Figure 24 and Figure 25 illustrate three snapshots of the scenario with their corresponding estimations, where the relative positions and orientations of the robots are represented by the inclined planes together with all particles.

We are still in the process of quantitatively analyzing the performance with the recorded real-time kinematic (RTK) ground-truth. However, we can see from the preliminary results that the estimated relative positions and orientations are in line with the scenario footage, which shows that the accuracy of the propagation time-based observations with the UWB devices is sufficiently high for swarm localization.

7. Conclusion

In this paper, we provide a complete solution for a self-organized swarm localization network employing low-cost and light-weight UWB devices. We start from evaluating the clock characteristics of the low-cost UWB devices. Then, we propose a SOTDMA scheme which is robust against network dynamics, packet loss, hidden node problems, etc. After that, we study localization-related observations from both active and passive nodes, accounting for the clock imperfection. We then design a decentralized algorithm for jointly estimating the relative position and orientation of the robots in a swarm. As one of the highlights, we successfully demonstrated our self-organized UWB swarm localization technology in a space-analogue surface exploration mission on the volcano Mt. Etna in July 2022. In this mission, a wheeled rover, a six-legged cave crawler and a hexacopter, each equipped with four UWB devices, performed coordinated exploration, while their positions and orientations are precisely estimated with our localization network. This paper provides a complete picture of our methods, system design and first results from the analogue mission, which sheds light on the usage of UWB for joint communication and navigation in a robotic swarm for future exploration missions.

Acknowledgments

Part of the presented research has been supported by the Helmholtz Association project Autonomous Robotic Networks to Help Modern Societies (ARCHES) (contract number ZT-0033), and the DLR projects Planetary Exploration and Swarm-Navigation.

References

[1] S. Zhang, R. Pöhlmann, T. Wiedemann, A. Dammann, H. Wymmeersch, and P. A. Hoeher, "Self-aware swarm navigation in autonomous exploration missions," *Proc. IEEE*, vol. 108, no. 7, pp. 1168–1195, 2020.

[2] E. Vassev, R. Sterritt, C. Rouff, and M. Hinchey, "Swarm technology at NASA: Building resilient systems," *IEEE IT Prof.*, vol. 14, no. 2, pp. 36–42, Mar. 2012.

[3] S. Zhang, E. Staudinger, R. Pöhlmann, and A. Dammann, "Cooperative communication, localization, sensing and control for autonomous robotic networks," in *IEEE International Conference on Autonomous Systems (IEEE ICAS 2021)*, August 2021. [Online]. Available: https://elib.dlr.de/142695/

[4] J. Degesys, I. Rose, A. Patel, and R. Nagpal, "DESYNC: Self-organizing desynchronization and TDMA on wireless sensor networks," in *2007 6th International Symposium on Information Processing in Sensor Networks*, 2007, pp. 11–20.

[5] D. Dardari, A. Conti, U. Ferner, A. Giorgetti, and M. Z. Win, "Ranging with ultrawide bandwidth signals in multipath environments," *Proc. IEEE*, vol. 97, no. 2, pp. 404–426, Feb. 2009.

[6] H. Wymeersch, J. Lien, and M. Win, "Cooperative localization in wireless networks," *Proc. IEEE*, vol. 97, no. 2, pp. 427–450, Feb. 2009.

[7] R. M. Buehrer, H. Wymeersch, and R. M. Vaghefi, "Collaborative sensor network localization: Algorithms and practical issues," *Proc. IEEE*, vol. 106, no. 6, pp. 1089–1114, Jun. 2018.

[8] S. Zhang, S. Sand, R. Raulefs, and E. Staudinger, "Self-organized hybrid channel access method for an interleaved RTD-based swarm navigation system," in *Proc. of 10-th Workshop on Positioning Navigation and Communication (WPNC)*, Dresden, Germany, Mar. 2013.

[9] S. Zhang, E. Staudinger, S. Sand, R. Raulefs, and A. Dammann, "Anchor-free localization using round-trip delay measurements for Martian swarm exploration," in *Proc. of IEEE ION PLANS*, Monterey, California, USA, May 2014.

[10] S. Zhang, E. Staudinger, T. Jost, W. Wang, C. Gentner, A. Dammann, H. Wymeersch, and P. A. Hoeher, "Distributed direct localization suitable for dense networks," *IEEE Trans. Aerosp. Electron. Syst.*, vol. 56, no. 2, pp. 1209–1227, 2020.

[11] S. Zhang, K. Cokona, R. Pöhlmann, E. Staudinger, T. Wiedemann, and A. Dammann, "Cooperative pose estimation in a robotic swarm: Framework, simulation and experimental results," in *2022 30th European Signal Processing Conference (EUSIPCO)*, 2022, pp. 987–991.

[12] E. Staudinger, S. Zhang, R. Poehlmann, and A. Dammann, "The role of time in a robotic swarm: A joint view on communications, localization, and sensing," *IEEE Commun. Mag.*, vol. 59, no. 2, pp. 98–104, 2021.

[13] S. Zhang, R. Pöhlmann, E. Staudinger, and A. Dammann, "Assembling a swarm navigation system: Communication, localization, sensing and control," in *2021 IEEE 18th Annual Consumer Communications Networking Conference (CCNC)*, 2021, pp. 1–9.

[14] A. Wedler *et al.*, "Finally! Insights into the ARCHES lunar planetary exploration analogue campaign on Etna in summer 2022," in *73. International Astronautical Congress (IAC), 18-23 September 2022*, September 2022.

[15] "IEEE standard for low-rate wireless networks," *IEEE Std 802.15.4-2020 (Revision of IEEE Std 802.15.4-2015)*, pp. 1–800, 2020.

[16] Y. Shen and M. Z. Win, "Fundamental limits of wideband localization - Part I: A general framework," *IEEE Trans. Inf. Theory*, vol. 56, no. 10, pp. 4956–4980, Oct. 2010.

[17] *DW1000 User Manual*, Decawave Ltd, 2017, version 2.18. [Online]. Available: https://www.qorvo.com/products/d/da007946

[18] T. Walter, "Characterizing frequency stability: a continuous power-law model with discrete sampling," *IEEE Transactions on Instrumentation and Measurement*, vol. 43, no. 1, pp. 69–79, 1994.

[19] M. B. Marinov, B. Ganev, N. Djermanova, and T. D. Tashev, "Analysis of sensors noise performance using allan deviation," in *2019 IEEE XXVIII International Scientific Conference Electronics (ET)*, 2019, pp. 1–4.

[20] E. Staudinger, S. Zhang, R. Pöhlmann, and A. Dammann, "The role of time in a robotic swarm: A joint view on communications, localization, and sensing," *IEEE Communications Magazine*, vol. 59, no. 2, pp. 98–104, 2021.

[21] R. Pagliari and A. Scaglione, "Scalable network synchronization with pulse-coupled oscillators," *IEEE Transactions on Mobile Computing*, vol. 10, no. 3, pp. 392–405, 2011.

BIOGRAPHY

Siwei Zhang *received his B.Sc. in electrical engineering from Zhejiang University, China, in 2009, his M.Sc. in communication engineering from the Technical University of Munich, Germany, in 2011, and his Dr.-Ing. (Ph.D.) in electrical engineering from the University of Kiel, Germany, in 2020. In 2012, he joined the Institute of Communications and Navigation of the German Aerospace Center (DLR) as a research staff member. His research interests lie in statistical signal processing in wireless communication and navigation, particularly in multi-agent joint communication, navigation and sensing. He is a recipient of the 2021 DLR Science Award.*

Pedro Fernandez Ruz *received a B.S. in Telecommunication Engineering from Malaga University in 2020. He has done research on mobile network optimization and embedded systems' development. During his six-month internship at the DLR, his master thesis focused on UWB ranging and localization and swarm-oriented network protocols.*

Fabio Broghammer *received the M.Sc. degree in Computer Science from the Karlsruhe Institute of Technology (KIT), Germany, in 2021. In 2022, he joined the Institute of Communications and Navigation of the German Aerospace Center (DLR) as a research staff member. His research interests include state estimation, swarm navigation and sensing.*

Emanuel Staudinger *received the M.Sc. degree in Embedded Systems Design from the University of Applied Sciences of Hagenberg, Austria, in 2010. Since 2010, he is with the Institute of Communications and Navigation of the German Aerospace Center (DLR), Wessling, Germany. He received a Ph.D. with distinction from the Institute of Electrodynamics and Microelectronics at the University of Bremen, Germany, in 2015. His current research interests include system design for cooperative positioning, experimental platform design based on SDRs, and experimental validation for swarm navigation. Within ARCHES he was responsible for the LOFAR mission design, and related system development for the radio-localization system, as well as proof of concept array operation.*

Christian Gentner *studied electrical engineering at the University of Applied Science in Ravensburg, with the main topic communication technology and received his Dipl.-Ing. (BA) degree in 2006. During this study he received practical experiences at Rohde & Schwarz in Munich. He continued his study at the University of Ulm in 2006. He received the M.Sc. and Dr.-Ing. (PhD) degree in 2009 and 2018 respectively, both from the University of Ulm. Since 2009, he is working at the Institute of Communications and Navigation of the German Aerospace Center (DLR). His current research focuses on multipath assisted and indoor positioning.*

Robert Pöhlmann *received the B.Sc. and the M.Sc. degrees in Electrical Engineering and Information Technology from the Technical University of Munich (TUM) in 2014 and 2016, respectively. In 2013 he joined the Institute of Communications and Navigation of the German Aerospace Center (DLR) as a student trainee and in 2016 he became a research staff member. His current research interests are in the area of statistical signal processing for multi-antenna systems and cooperative localization.*

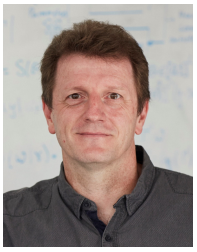

Armin Dammann *received the Dipl.-Ing. (M.Sc.) and Dr.-Ing. (Ph.D.) degrees in Electrical Engineering from the University of Ulm, Germany, in 1997 and 2005 respectively. In 1997 he joined the Institute of Communications and Navigation of the German Aerospace Center (DLR) as a research staff member. Since 2005 he is head of the Mobile Radio Transmission Research Group. His research interest and activities include signal design and signal processing for terrestrial wireless communication and navigation systems. In these fields, he has been active in several EU-projects, e.g., WINNER, WHERE and WHERE2. Armin Dammann is lecturer at the Technical University of Munich for* Robot and Swarm Navigation.

Manuel Schütt *received his MA Sc. degree in Photonics at Hochschule München. He is currently working as a research associate at the Institute of System Dynamics and Control of the German Aerospace Center (DLR). His main research interest is terramechanics and ground behaviors detection .Currently he is developing the Scout rover to explore lunar and martian lava tubes by 2030.*

Roy Lichtenheldt *received his Dr.-Ing. degree in Mechatronics at TU Ilmenau. He is currently working as a research associate at the Institute of System Dynamics and Control of the German Aerospace Center (DLR). His main research interest is terramechanics and innovative locomotion systems. Currently he is leading a group developing the Scout rover to explore lunar and martian lava tubes by 2030. Within the MMX mission, he leads the development of the rover's wheels.*